The dependence of the coupled magnetosphere-ionosphere-thermosphere system on the Earth's magnetic dipole moment

Ingrid Cnossen,[1] Arthur D. Richmond,[1] and Michael Wiltberger[1]

Received 23 January 2012; revised 27 February 2012; accepted 19 March 2012; published 3 May 2012.

[1] The strength of the Earth's magnetic field changes over time. We use simulations with the Coupled Magnetosphere-Ionosphere-Thermosphere model to investigate how the magnetosphere, upper atmosphere, and solar quiet (Sq) geomagnetic variation respond as the geomagnetic dipole moment M varies between $2 \cdot 10^{22}$ and $10 \cdot 10^{22}$ Am^2. We find that the magnetopause stand-off distance and the cross-polar cap potential increase, while the polar cap size decreases, with increasing M. Their dependence on M is stronger than predicted by previous studies. We also show for the first time that the shape of the magnetosphere starts to change for $M \leq 4 \cdot 10^{22}$ Am^2. This may be due to enhanced magnetopause erosion and/or to strong changes in the ionospheric conductance, which affect the field-aligned currents and the magnetic fields they create in the magnetosphere, thus modifying the magnetic pressure inside the magnetosphere. $\mathbf{E} \times \mathbf{B}$ drift velocities, Joule heating power, the global mean thermospheric temperature and the global mean height of the peak of the ionospheric F_2 layer, h_mF_2, all increase with increasing M for low dipole moments, but all decrease with increasing M for larger dipole moments. The peak electron density of the F_2 layer, N_mF_2, shows the opposite behavior. The Sq amplitude decreases with increasing M and this dependence can be roughly described by a power law scaling. Most scaling relations show a weak dependence on the solar activity level, which is likely associated with a change in the relative contributions to the Pedersen conductance from the upper and lower ionosphere, which scale differently with M.

Citation: Cnossen, I., A. D. Richmond, and M. Wiltberger (2012), The dependence of the coupled magnetosphere-ionosphere-thermosphere system on the Earth's magnetic dipole moment, *J. Geophys. Res.*, *117*, A05302, doi:10.1029/2012JA017555.

1. Introduction

[2] The Earth's magnetic field strength changes over time. Over the past 800,000 years the geomagnetic dipole moment has fluctuated between values of $\sim 1 \cdot 10^{22}$ Am^2 to $\sim 10 \cdot 10^{22}$ Am^2 [*Guyodo and Valet*, 1999], with the current value being approximately $7.7 \cdot 10^{22}$ Am^2. While the present-day magnetic field is relatively strong in a geological context, the dipole moment has been steadily decreasing since $\sim$1840 at a rate of 5–7% per century [*Mandea and Purucker*, 2005; *Gubbins et al.*, 2006]. If this declining trend continues, we can thus expect a considerably weaker magnetic field over centuries to come.

[3] A change in the Earth's magnetic field strength has consequences for the magnetosphere-ionosphere-thermosphere (MIT) system. Previous work has indicated that magnetic field changes may be responsible for up to 30% of trends that have been observed in the ionospheric F_2 layer over the past $\sim$50 years [*Cnossen and Richmond*, 2008]. Long-term trends that have been observed in the solar quiet (Sq) geomagnetic variation [*Macmillan and Droujinina*, 2007; *Elias et al.*, 2010] may also be partially caused by magnetic field changes. However, it can be difficult to understand exactly how historical magnetic field changes have influenced the upper atmosphere, as changes in strength and orientation occur simultaneously, and can also vary strongly with location. It is therefore useful to isolate the role of the dipole moment.

[4] A number of studies have considered how magnetospheric variables are expected to change as a function of the geomagnetic dipole strength. Considering the pressure balance at the magnetopause between the solar wind dynamic pressure and the magnetic pressure from the Earth's magnetic field, it can be found that the stand-off distance R_s should scale as $R_s \propto M^{1/3}$ [e.g., *Kivelson and Russell*, 1995]. From this initial scaling relation, *Siscoe and Chen* [1975] and *Glassmeier et al.* [2004] derived further theoretical scalings for other magnetospheric variables based on the main assumption of "self-similarity," i.e., no change in the shape of the magnetosphere.

[5] *Zieger et al.* [2006a, 2006b] used the analytical Hill-Siscoe model [*Hill et al.*, 1976; *Siscoe et al.*, 2002a, 2002b]

[1]High Altitude Observatory, National Center for Atmospheric Research, Boulder, Colorado, USA.

Corresponding Author: I. Cnossen, High Altitude Observatory, National Center for Atmospheric Research, 3080 Center Green Dr., Boulder, CO 80301, USA. (icnossen@ucar.edu)

0148-0227/12/2012JA017555

and the BATS-R-U.S. MHD model to verify these theoretical scaling relations. They suggested some modifications, mainly a dependence of the scaling with M on the B_z component of the Interplanetary Magnetic Field (IMF), but they did not find any significant deviation from self-similarity. A weakness in their approach was that their model did not include the ionosphere, and instead assumed a constant, uniform conductance as the inner boundary condition for the magnetospheric simulations. This conductance was manually adjusted for each simulation according to $\Sigma_P \propto M^{-1}$, following *Glassmeier et al.* [2004].

[6] *Cnossen et al.* [2011] were the first to study the effects of a reduction in magnetic field strength on the coupled MIT system, calculating changes in ionospheric conductance self-consistently as part of their simulations with the Coupled Magnetosphere-Ionosphere-Thermosphere (CMIT) model. Based on two simulations with dipole moments of $6 \cdot 10^{22}$ and $8 \cdot 10^{22}$ Am^2, they inferred that the dayside Pedersen and Hall conductances depend on the dipole moment as $\Sigma_P \propto M^{-1.5}$ and as $\Sigma_H \propto M^{-1.7}$, i.e., much more strongly than assumed in previous studies. They also showed for the first time the response of the ionosphere and thermosphere to a 25% reduction in dipole moment.

[7] Here we extend the work done by *Cnossen et al.* [2011] by considering a larger range of dipole moments and examining how a number of MIT parameters vary as a function of this. We also investigate the influence of the solar activity level. This changes the ionospheric conductance, which may modify the response of the MIT system to a change in dipole moment. Where possible we compare our findings to theoretical scaling relations and scaling relations derived by the MHD modeling studies mentioned above. The aim of the present study is to provide a better insight in the role of the geomagnetic dipole strength in the behavior of the MIT system. This is interesting in its own right, but also relevant from a geological perspective [see, e.g., *Tarduno et al.*, 2010], and it serves as a basis for the interpretation of the effects of the complex magnetic field changes that have occurred in the last ~50–100 years.

[8] This paper is organized as follows. In section 2 we describe the CMIT model and the settings used specifically for the simulations in our study. In section 3 we show how a range of variables depend on the dipole moment, starting with the magnetosphere and high-latitude ionosphere, then the global mean ionosphere and thermosphere, and finishing with the Sq variation. This is followed by a discussion of the results in section 4, and a summary and conclusions in section 5.

2. Methodology

2.1. Model Description

[9] We examine the effects of changes in the geomagnetic dipole moment using the Coupled Magnetosphere-Ionosphere-Thermosphere (CMIT) model [*Wiltberger et al.*, 2004; *Wang et al.*, 2004, 2008]. CMIT couples the Lyon-Fedder-Mobarry (LFM) global magnetospheric code [*Lyon et al.*, 2004] with the Thermosphere-Ionosphere-Electrodynamics General Circulation Model (TIE-GCM) [*Roble et al.*, 1988; *Richmond et al.*, 1992] through the MIX coupler solver module [*Merkin and Lyon*, 2010].

[10] The LFM component of the model solves the ideal magnetohydrodynamic (MHD) equations to simulate the interaction between the solar wind and the magnetosphere and calculates the full MHD state vector (plasma density, pressure, velocity and magnetic field). It requires the solar wind MHD state vector on its outer boundary as input and uses an empirical parameterization [*Wiltberger et al.*, 2009] to calculate the energy flux of precipitating electrons. On its inner boundary it requires the ionospheric conductance to calculate the electric potential, which is passed in from the TIE-GCM part of the code through the MIX module.

[11] The TIE-GCM is a time dependent, three-dimensional model that solves the fully coupled, nonlinear, hydrodynamic, thermodynamic, and continuity equations of the thermospheric neutral gas self-consistently with the ion continuity equations. At high latitudes it requires the auroral particle precipitation and electric field imposed from the magnetosphere, which it receives from the MIX component of the code. The solar activity level is specified through an F10.7 value.

[12] The coupling of the LFM and TIE-GCM in CMIT enables the calculation of the global ionospheric electric field, which includes both the imposed high latitude electric field from the magnetosphere and the dynamo electric fields generated by thermospheric winds. This makes CMIT a two-way coupled model, in which the magnetosphere is able to influence the ionosphere-thermosphere system and vice versa. As we shall see, this is important when studying the effects of changes in the Earth's magnetic field.

2.2. Simulation Setup and Analysis

[13] For our simulations we specified the Earth's magnetic field as a dipole, with the position of the geomagnetic pole in the northern hemisphere fixed at 80°N and 70°W, following *Cnossen et al.* [2011]. Simulations were performed with five different dipole strengths of $2 \cdot 10^{22}$, $4 \cdot 10^{22}$, $6 \cdot 10^{22}$, $8 \cdot 10^{22}$ and $10 \cdot 10^{22}$ Am^2, which we will refer to as M2, M4, M6, M8, and M10, respectively, and three different solar activity levels (F10.7 of 80, 150 and 220), which we will refer to as solar minimum (smin), solar medium (smed) and solar maximum (smax).

[14] All simulations were done for a period of 36 h, starting at 0 UT on 21 March (equinox), and used the same idealized solar wind conditions. The solar wind density was set to a constant value of 5 cm^{-3}, and the outward solar wind speed was set to 400 km/s, while the speed in the geocentric solar magnetospheric (GSM) y- and z-direction was set to zero. The B_z component of the IMF was set to −5 nT for the first two hours (0–2 UT), +5 nT for the second two hours (2–4 UT), and −5 nT for the rest of the simulation, while the B_x and B_y components were set to zero for the full duration of the simulations. The IMF components are defined in GSM coordinates. The sound speed of the plasma in the solar wind was set to a constant 40 km/s, ensuring that the incoming solar wind was highly supersonic. These settings are the same as used by *Cnossen et al.* [2011].

[15] Only the last 24 h of each simulation were used for analysis since the first 12 h are required to reach a quasi-steady state. Most results are presented in the form of a mean with standard deviation over the last 24 h. With data output every 6 min, this gives 240 values for each calculation. To

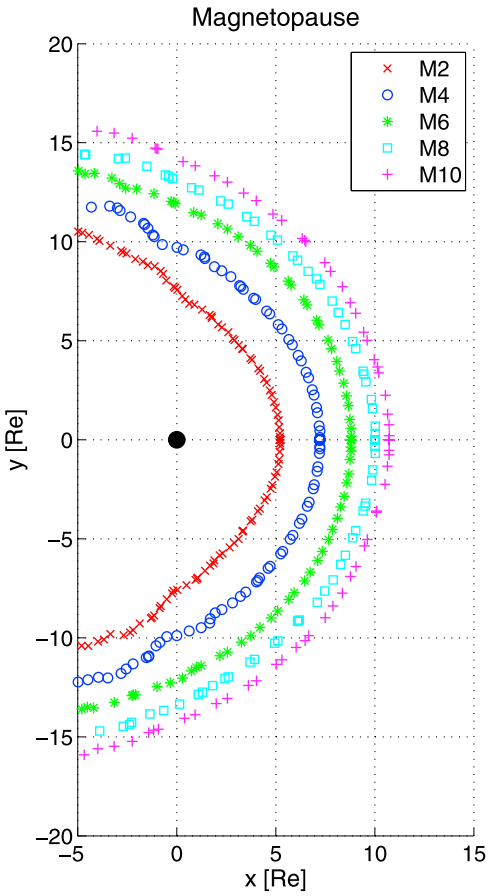

Figure 1. The magnetopause for the M2, M4, M6, M8, and M10 simulations, all for solar medium conditions.

describe how a given variable scales with the dipole moment, we fitted power law scaling relations to the data points where appropriate (i.e., when the fit was clearly very poor, this was omitted). All power law scalings found are noted in the relevant figures and summarized in Table 1 in section 5.

3. Results

3.1. The Magnetosphere and High-Latitude Ionosphere

[16] The size of the Earth's magnetosphere is to first order determined by the pressure balance between the magnetic pressure inside the magnetosphere and the solar wind dynamic pressure on the outside. The magnetosphere is thus expected to shrink as the geomagnetic field strength decreases. This is confirmed by Figure 1, which shows the magnetopause for the M2, M4, M6, M8 and M10 simulations for solar medium conditions.

[17] Figure 2 (top) shows how the stand-off distance (the distance from the center of the Earth to the magnetopause at the sub-solar point) R_s varies as a function of dipole moment for all three solar activity levels. Power law fits to these data points and the theoretical relationship $R_s \propto M^{1/3}$ are also shown. The theoretical curve was constrained to go through the M8-smed value calculated by the model. Although the theoretical relationship works reasonably well in the vicinity of M8-smed, the model results clearly show a stronger dependence of R_s on M. The dependence is also slightly stronger for higher solar activity, but the differences between different solar activity levels are not statistically significant.

[18] Figure 2 (bottom) shows the ratio between the average distance to the magnetopause in the y-direction (i.e., to the flank of the magnetosphere) from the center of the Earth and the stand-off distance. This is a measure of the shape of the magnetosphere, which we use to test whether the magnetosphere remains self-similar for different dipole strengths. We find that this is more or less the case for M6, M8 and M10. However, for M4 the flank/nose distance ratio becomes slightly larger, and for M2 the ratio is clearly significantly larger than for all other cases. This means that the magnetosphere is no longer purely self-similar for extreme changes in dipole moment. The departure from self-similarity is stronger for higher solar activity level. The change in shape can also be seen in Figure 1, although it is not directly obvious. Still, when focusing on the magnetopause boundaries for M2 and M10, one can notice that the M10 magnetosphere is more rounded, while the M2 magnetosphere has a sharper (more pointed) nose and opens outwards more on the flanks. In other words, the flaring angle is larger for smaller dipole moments.

[19] We have identified two possible contributors to the deviation of the modeled stand-off distances from the theoretical relationship and the change in the shape of the magnetosphere for large changes in dipole moment. The first is the effect of magnetopause erosion on the stand-off distance. An increase in the southward component of the IMF normally results in an enhanced reconnection rate, which reduces the stand-off distance through the erosion of closed field lines [e.g., *Wiltberger et al.*, 2003]. A similar effect can be expected when the dipole moment is decreased for a constant southward IMF, as is done here. As the dipole moment is reduced, the stand-off distance would thus decrease further than expected from theory and would also decrease more than the distance to the magnetopause on the flanks, producing the change in shape of the magnetopause. A second potential contributor is associated with changes in the field-aligned currents (see Figure 3). *Siscoe et al.* [2002b] noted that field-aligned currents play a secondary role in the magnetopause pressure balance in today's magnetosphere. A field-aligned current loop that arises on the dayside of the magnetosphere, consisting of a dawnward current across the noon-meridian plane, produces a magnetic field in the negative z-direction. This opposes the Earth's main magnetic field, thus diminishing the magnetic pressure inside the magnetopause on the dayside, and reducing the stand-off distance. In contrast, on the flanks of the magnetosphere, the field-aligned current loops are oriented in such a way that they enhance the magnetic pressure inside the magnetosphere, and thereby increase the size of the magnetosphere in the y-direction [*Merkin et al.*, 2005]. *Merkin et al.* [2005] showed that both effects exist in the LFM and become stronger as the field-aligned currents become stronger. Figure 3 indicates that the total field-aligned current increases with decreasing dipole moment. By the mechanism outlined above, this thus results in a reduction of the stand-off distance, in addition to the reduction expected from the theoretical scaling relation, while it offsets some of the overall reduction in magnetosphere size on the flanks, as the dipole moment decreases.

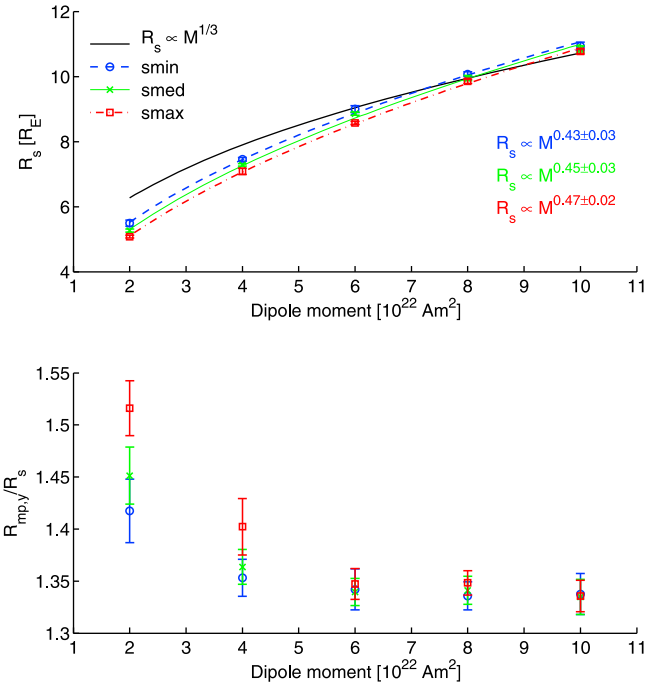

Figure 2. The (top) stand-off distance R_s and (bottom) flank/nose distance ratio of the magnetopause as a function of dipole moment for three different solar activity levels. Each value is a 24-h average, with the standard deviation indicated by error bars. Power law fits to the R_s data points are also shown, as well as the theoretical scaling relation $R_s \propto M^{1/3}$. The latter was constrained such that the theoretical value agrees with the modeled value for M8-smed. The upper/lower limits on the power law scaling coefficients represent the 95% confidence interval.

[20] The changes in the field-aligned currents are caused by changes in ionospheric conductance: the higher the conductance, the stronger the field-aligned currents will be for a given electric potential. The ionospheric conductance depends directly on the magnetic field strength, partly through the effect of the field strength on the gyrofrequencies [e.g., *Richmond*, 1995]. The global mean ionospheric conductance as a function of dipole moment is shown in Figure 4. Differences between day and night are averaged out this way, but we note that the largest changes occur on the dayside, as was shown by *Cnossen et al.* [2011]. The dependence of the global mean ionospheric conductance on the dipole moment can be described quite well by power law scaling relations. The scaling of the Pedersen conductance depends slightly on the solar activity level, being strongest for the highest solar activity level, while such dependence is not significant for the Hall conductance.

[21] As the ionospheric conductance changes, not only the field-aligned currents, but also the electric potential changes. Figure 5 shows the cross-polar cap potential as a function of dipole moment. *Glassmeier et al.* [2004] argued that the cross-polar cap potential Φ should scale as the extent of the magnetopause reconnection region, and that this in turn should scale in the same way as the stand-off distance. Assuming $R_s \propto M^{1/3}$, they obtained the theoretical scaling $\Phi \propto M^{1/3}$. This relation is also shown in Figure 5, constrained to go through the M8-smed point calculated by the model. Given that we already found that the stand-off distance does not quite follow $R_s \propto M^{1/3}$, it is not surprising that the modeled cross-polar cap potential values deviate considerably from the theoretical scaling for large changes in M. However, we find that the cross-polar cap potential does in fact not even obey a power law of the form $\Phi \propto M^{\gamma}$. This indicates that it does not scale in the same way as R_s, which means that the assumptions made by *Glassmeier et al.* [2004] are not entirely correct. This will be further discussed in section 4.1.

[22] To find out what happens to the electric field at high latitudes, not only the change in cross-polar cap potential, but also the change in the size of the polar cap must be considered. The overall reduction in the size of the magnetosphere for decreasing dipole strength means that the last closed field lines map to lower geomagnetic latitudes, increasing the size of the polar cap. Based on the $R_s \propto M^{1/3}$ scaling for the stand-off distance and assuming a self-similar magnetosphere, *Siscoe and Chen* [1975] argued that $\cos \lambda_{pc} \propto M^{-1/6}$, where λ_{pc} is the magnetic latitude of the polar cap boundary. Again, we find a somewhat stronger relationship, as shown in Figure 6. The data points roughly fit the power laws indicated, but the fits are clearly not perfect.

[23] The increase in polar cap size and decrease in cross-polar cap potential with decreasing dipole strength both act to reduce the high-latitude electric field E. A change in the electric field affects the ion $\mathbf{E} \times \mathbf{B}$ drifts, which scale as E/B. To obtain a measure of the change in $\mathbf{E} \times \mathbf{B}$ drift velocities, we approximate E as $\Phi/\cos \lambda_{pc}$ and divide this by M in units of 10^{22} Am^2. This quantity is plotted in Figure 7 (top) as a function of M. Starting from M2, the measure of E/B initially increases with increasing M, which means that E increases more rapidly than B. However, as M increases further, this relationship changes, and E/B decreases with increasing M. The switchover point occurs at larger M for higher solar activity and the changes are in general stronger for higher solar activity. This behavior can also be identified in the $\mathbf{E} \times \mathbf{B}$ drift patterns themselves (not shown), and it is

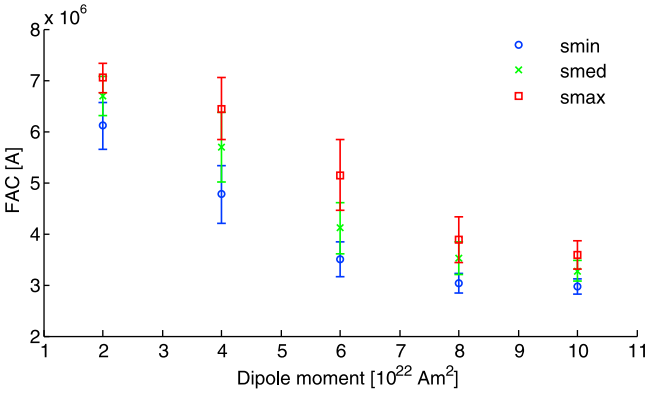

Figure 3. The integrated vertical current going into and out of the ionosphere averaged between both hemispheres as a function of dipole moment for three different solar activity levels. Each value is a 24-h average, with the standard deviation indicated by error bars.

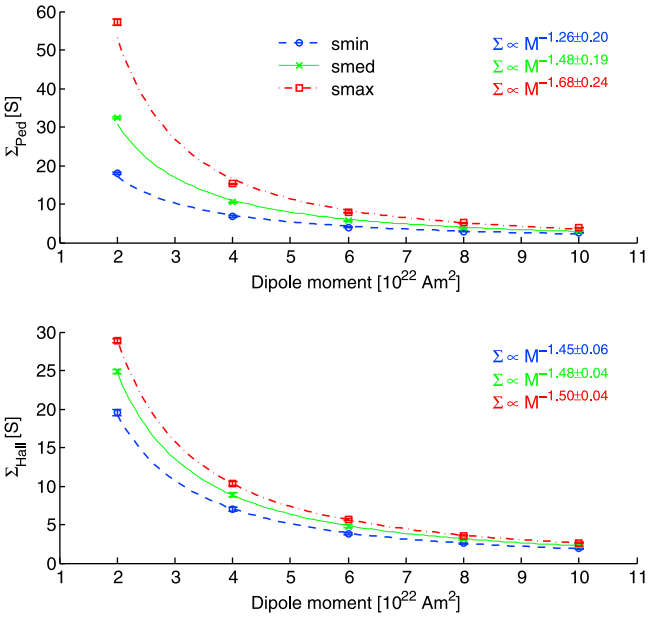

Figure 4. The mean (top) Pedersen and (bottom) Hall conductance averaged over both hemispheres as a function of dipole moment for three different solar activity levels. Each value is a 24-h average, with the standard deviation indicated by error bars. Power law fits to the data points are also shown, with limits on the scaling coefficients representing the 95% confidence interval.

obvious in the Joule heating power too, shown in Figure 7 (bottom).

3.2. The Global Mean Ionosphere and Thermosphere

[24] The high-latitude changes in **E** × **B** drifts and Joule heating cause further changes to global circulation patterns and the neutral temperature structure. *Cnossen et al.* [2011] showed detailed patterns of change between the M6 and M8 smed simulations. Here we will consider global mean quantities only. Figure 8 shows the global mean neutral temperature and electron density profiles for the M2, M4, M6, M8 and M10 simulations for solar medium conditions. The global mean temperature changes with the dipole moment in a similar way as the Joule heating: it increases with increasing M for very low M, but decreases with increasing M for larger M. This can be seen more clearly in Figure 9 (top), which shows the change in exospheric temperature as a function of dipole moment for all three solar activity levels.

[25] Figure 9 (middle) shows the global mean peak electron density of the F_2 layer, N_mF_2, as a function of dipole moment. This variable appears to behave in the opposite sense to the global mean neutral temperature. By comparing the global patterns of change between M6 and M8, *Cnossen et al.* [2011] showed that changes in electron density could be linked to changes in the O/N_2 ratio, a measure of ion production versus ion loss. We find that this is again the case here. The changes in O/N_2 ratio themselves are caused by changes in the neutral circulation. As the Joule heating increases, temperatures at high latitudes increase, so that more upwelling takes place. This brings more molecular-rich air upwards, resulting in a decrease of the O/N_2 ratio, and

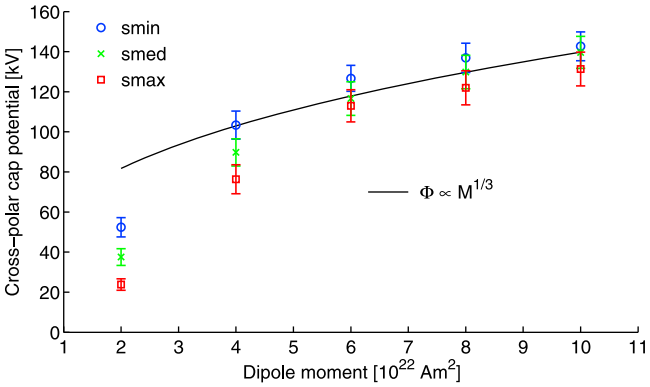

Figure 5. The cross-polar cap potential averaged between both hemispheres as a function of dipole moment for three different solar activity levels. Each value is a 24-h average, with the standard deviation indicated by error bars. The theoretical scaling relation of the cross-polar cap potential Φ with dipole moment M, $\Phi \propto M^{1/3}$, is also shown, with the constraint that the theoretical value agrees with the modeled value for M8-smed.

hence a decrease in electron density. The opposite takes place when the Joule heating decreases. The changes in N_mF_2 are therefore always in the opposite sense of the changes in Joule heating and global mean neutral temperature.

[26] The global mean height of the peak of the F_2 layer, h_mF_2, shown in Figure 9 (bottom), behaves roughly similarly to the global mean neutral temperature, but does not exactly match it. The changes in the global mean h_mF_2 are therefore likely to be partly due to the thermal expansion/contraction of the thermosphere as the neutral temperature changes, but other effects could play a role also. For instance, changes in the transport of ionospheric plasma by neutral winds up or down magnetic field lines, into regions of weaker or stronger recombination, respectively, could also affect the global mean electron density profile.

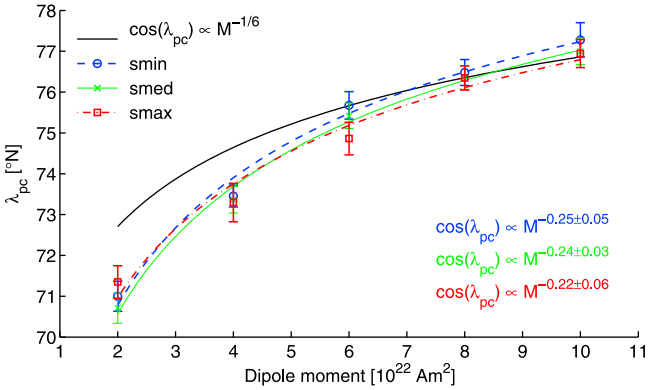

Figure 6. The magnetic latitude of the polar cap boundary, λ_{pc}, as a function of dipole moment for three different solar activity levels. Each value is a 24-h average, with the standard deviation indicated by error bars. The theoretical curve, obtained from the theoretical relation $\cos \lambda_{pc} \propto M^{-1/6}$, is also shown, with the constraint that the theoretical value agrees with the modeled value for M8-smed. Power law fits to the data points are also shown, with limits on the scaling coefficients representing the 95% confidence interval.

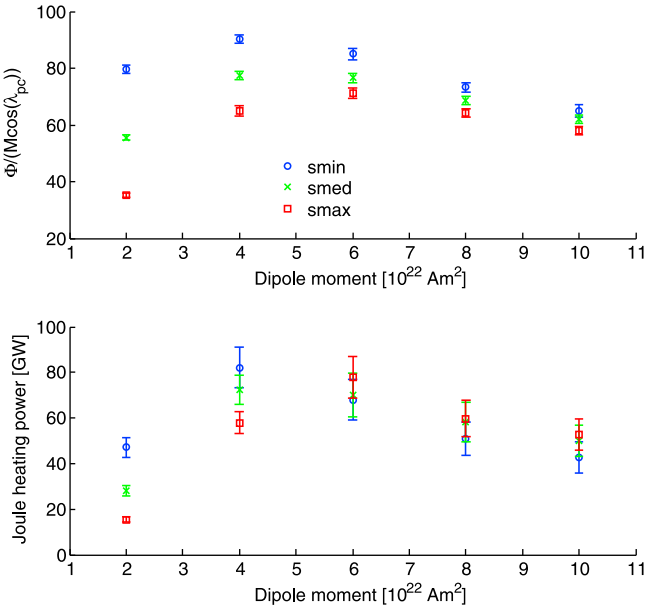

Figure 7. The cross-polar cap potential Φ divided by (top) $M\cdot\cos\lambda_{pc}$ (a measure of E/B) and (bottom) the Joule heating power as a function of dipole moment for three different solar activity levels. Each value is a 24-h average, with the standard deviation indicated by error bars.

3.3. The Solar Quiet (Sq) Geomagnetic Variation

[27] The current system responsible for the solar quiet (Sq) variation in geomagnetic activity, observed at the ground at low to midlatitudes, depends on the ionospheric conductance and neutral winds. Changes in the dipole moment can therefore be expected to change the amplitude of the Sq variation. Since we have steady solar wind conditions (no substorms), we obtain a clear daily variation in geomagnetic perturbations in all three components, which we interpret as Sq variation. We take the difference between the maximum and minimum perturbation at a given location over the last 24 h of the simulations as a measure of the Sq amplitude. In this case we average over all longitudes to obtain a mean and standard deviation. The Sq amplitude at 30° magnetic latitude calculated in this way is shown as a function of dipole moment in Figure 10.

[28] The Sq amplitude of all three components decreases with increasing dipole moment. It is possible to capture this behavior by power law fits over the entire dipole moment range, but we found that this resulted in relatively large confidence intervals and poor fits. This was mainly due to the M2 data points not fitting in very well (a behavior seen previously for other variables too). We therefore excluded the M2 data points from the fitting procedure in this case, and the scaling relations shown in Figure 10 are thus only valid for the range M4-M10. The scaling for solar maximum still has relatively large confidence limits, which is probably due to the M4 data point already starting to behave differently as well for higher solar activity. There is a weak dependence of the scaling relations themselves on the solar activity level, with the dependence on M being somewhat stronger for lower solar activity, but this is only significant for the northward component when comparing solar minimum to solar medium conditions. The dependence of the northward Sq component on M is also somewhat sensitive to the exact magnetic latitude chosen: it gets stronger for 35° magnetic latitude and weaker for 25° magnetic latitude (not shown). The scaling relations for the eastward and downward component on the other hand are quite robust with respect to magnetic latitude.

4. Discussion

4.1. Comparison With Previous Studies

[29] Our results show that the theoretical scaling for the stand-off distance, $R_s \propto M^{1/3}$, is too weak. This is due to a strong increase of the ionospheric conductance with decreasing dipole moment, which leads to a strengthening of the field-aligned currents. The magnetic fields generated by these currents oppose the main field on the nose of the magnetosphere, while they add to it on the flanks. The nose of the magnetosphere is therefore compressed more with diminishing dipole strength than expected from $R_s \propto M^{1/3}$, while the flanks are compressed less than expected. Previous modeling studies [e.g., *Zieger et al.*, 2006a, 2006b] did not incorporate a fully coupled ionosphere, and therefore missed

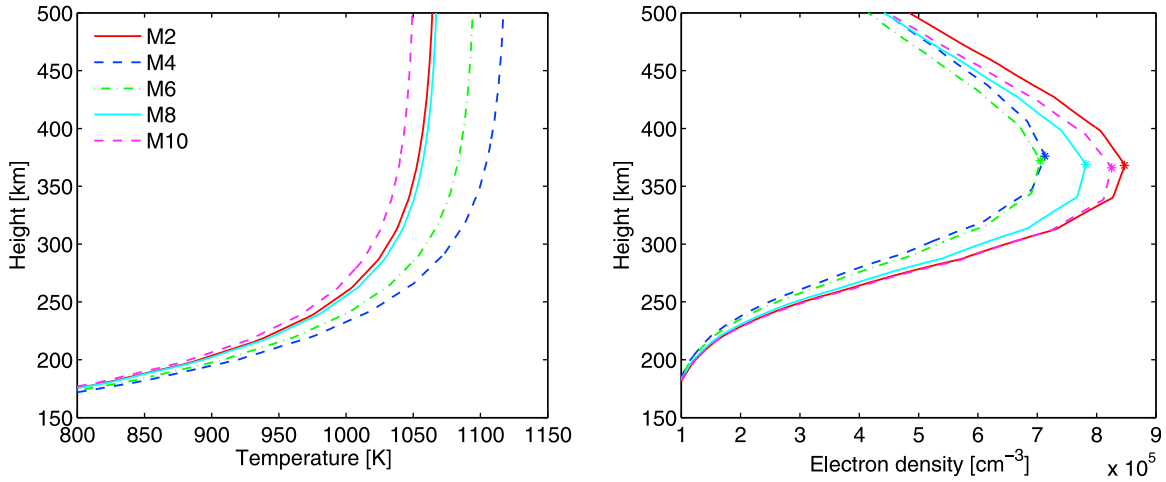

Figure 8. Global mean temperature and electron density profiles for M2, M4, M6, M8, and M10, all for solar medium conditions.

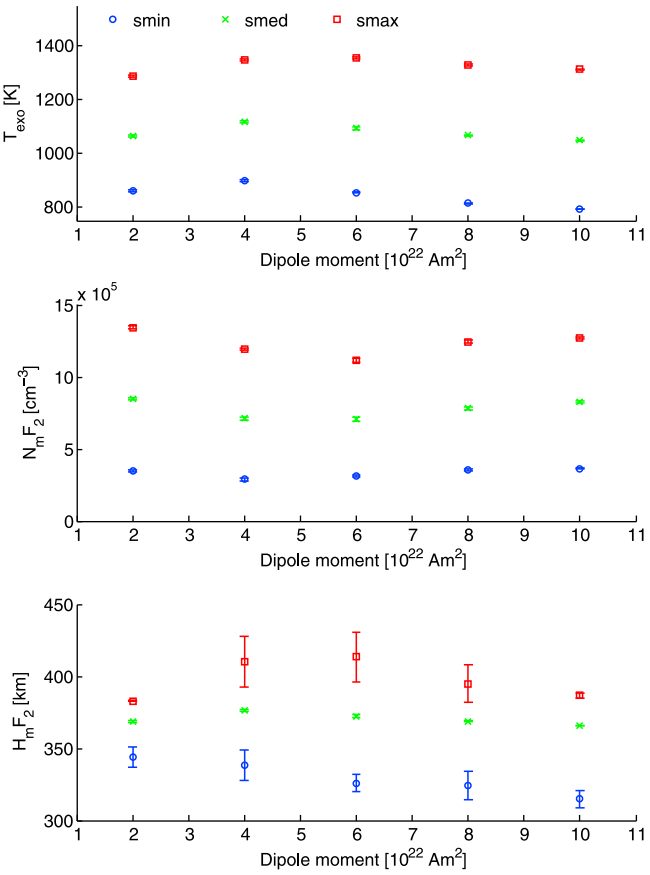

Figure 9. The (top) global mean exospheric temperature, (middle) peak electron density of the F_2 layer, N_mF_2 and (bottom) height of the F_2 peak, h_mF_2 as a function of dipole moment for three different solar activity levels. Each value is a 24-h average, with the standard deviation indicated by error bars.

this effect. Since the $R_s \propto M^{1/3}$ scaling forms the basis for many other scaling relations, these are all likely to show a too weak dependence on M as well. This is for instance what we see in the scaling for the low-latitude boundary of the polar cap and the cross-polar cap potential.

[30] There may be an additional issue with the theoretical scaling for the cross-polar cap potential derived by *Glassmeier et al.* [2004]. They argued that the cross-polar cap potential should depend on the extent of the dayside reconnection region, and that this should in turn scale as the stand-off distance. We find that the cross-polar cap potential does not obey a power law dependence on M, while the stand-off distance does, meaning that there must be something wrong with the assumptions. It does seem reasonable that the dayside reconnection region should scale as the stand-off distance, although the change in the shape of the magnetosphere could potentially alter this somewhat. However, the main problem may lie in the assumption that the cross-polar cap potential scales as the extent of the reconnection region. A recent study with the stand-alone LFM indicates that this is not the case, due to the influence of viscous processes, which also affect the cross-polar cap potential (R. E. Lopez, personal communication, 2011). Also, the reconnection rate might not stay constant for very small dipole moments. A simple power law scaling for the cross-polar cap potential can therefore not be obtained.

4.2. Solar Activity Dependence

[31] The ionospheric conductance depends on the solar activity level, as can be clearly seen in Figure 3. For that reason it is perhaps not surprising that the scaling of the Pedersen conductance with M depends somewhat on the solar activity level, with the scaling being stronger for higher solar activity. However, such solar activity influence is largely absent for the Hall conductance scaling with M. To explain this, we have to examine the factors that influence the Pedersen conductance more closely.

[32] The Pedersen conductivity is given by [e.g., *Richmond*, 1995]:

$$\sigma_P = \frac{N_e e}{B}\left(\frac{\nu_{in}\Omega_i}{\nu_{in}^2+\Omega_i^2}+\frac{\nu_{en\perp}\Omega_e}{\nu_{en\perp}^2+\Omega_e^2}\right) \quad (1)$$

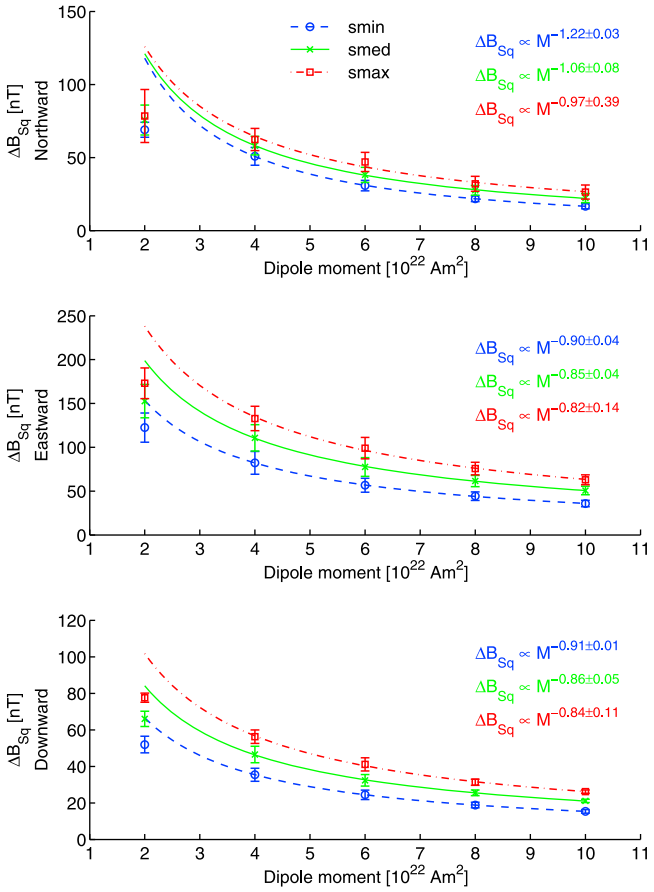

Figure 10. The Sq amplitude of the (top) northward, (middle) eastward and (bottom) downward components at 30° magnetic latitude as a function of dipole moment for three different solar activity levels. Each value is an average over all longitudes and both hemispheres, with the standard deviation indicated by error bars. Power law fits to the data points are also shown, with limits on the scaling coefficients representing the 95% confidence interval. Note that the M2 data points were excluded when deriving these fits. The scaling coefficients are thus valid only for the range M4-M10.

where σ_P = Pedersen conductivity, N_e = electron number density, e = magnitude of the electron charge, B = magnitude of the magnetic field, ν_{in} = collision frequency of ions with neutrals, $\nu_{en\perp}$ = collision frequency of electrons with neutrals in the direction perpendicular to the magnetic field, Ω_i = ion gyrofrequency, and Ω_e = electron gyrofrequency. The ion and electron gyrofrequencies are in turn given by:

$$\Omega_i = eB/m_i \tag{2a}$$

$$\Omega_e = eB/m_e \tag{2b}$$

where m_i = ion mass, and m_e = electron mass. In the F_2 layer ionosphere, the collision frequencies are much smaller than the gyrofrequencies. It follows from equations (1) and (2) that in this limit the Pedersen conductivity scales with the magnetic field strength as $\sigma_P \propto M^{-2}$. In contrast, in the lower ionosphere, the collision frequencies are much larger than the gyrofrequencies. In this case there is no direct dependence of the Pedersen conductivity on the magnetic field strength. The dependence of the height-integrated Pedersen conductivity (i.e., the Pedersen conductance) on the magnetic field strength lies somewhere in between these extremes.

[33] The solar activity dependence of the scaling of Σ_P with M arises from a shift in the balance between contributions to Σ_P from the lower and upper ionosphere. During solar maximum conditions, the F_2 layer contributes relatively more to the Pedersen conductance [*Richmond*, 1995]. This brings the scaling relation closer to $\Sigma_P \propto M^{-2}$ for higher solar activity. The Hall conductance on the other hand always peaks in the E region, regardless of the solar activity level [*Richmond*, 1995]. Changes in solar activity do therefore not significantly affect the scaling of the Hall conductance with M.

[34] The ionospheric conductance plays a crucial role in the response of the MIT system as a whole to the changes in dipole moment. Most other variables thus exhibit some dependence on the solar activity level in their scaling with M, and in most cases the scaling is stronger for higher solar activity level, as it is for the Pedersen conductance. Only the Sq amplitudes clearly show the opposite behavior, with scaling laws becoming weaker for higher solar activity. Why this weakened scaling at higher solar activity occurs is not immediately obvious. A simple model that considers Sq to scale as the product of the conductances and the magnetic field strength (because of the dependence of wind-driven current on $\mathbf{U} \times \mathbf{B}$) would predict the inverse scaling dependence of Sq on M to be stronger at solar maximum. However, the development of a polarization electric field in the ionosphere that ensures current closure depends to some extent on the ratio of Hall to Pedersen conductances: a higher ratio will tend to produce a stronger polarization electric field and therefore a stronger Sq current. From the scaling relations derived in Figure 4 it can easily be seen that the Hall to Pedersen conductance ratio has a positive dependence on M at solar maximum, but a negative dependence on M at solar minimum. The positive dependence at solar maximum thus tends to reduce the overall inverse dependence of Sq currents on M at solar maximum, while the negative dependence at solar minimum adds to the overall inverse dependence.

4.3. Implications for Long-Term Trend Studies

[35] The scaling relations obtained here may be used in future work to estimate the steady state of the magnetosphere and upper atmosphere for any time in the past when the Earth's dipole moment was different. We intend to use the results to estimate to what extent changes in the magnetic field strength may have contributed to the observed decadal to century-scale trends in the upper atmosphere and the Sq variation.

[36] From 1910 to 2010, the geomagnetic dipole moment changed from $\sim 8.3 \cdot 10^{22}$ Am^2 to $\sim 7.7 \cdot 10^{22}$ Am^2 (based on the International Geomagnetic Reference Field [*Finlay et al.*, 2010]). We estimate the change in global mean exospheric temperature and global mean h_mF_2 between 1910 and 2010 due to the change in dipole moment through interpolation from straight-line fits to the M6, M8 and M10 data points. This gives an increase in global mean exospheric temperature of 6–9 K and an increase in global mean h_mF_2 of 1–4 km.

[37] Since the thermosphere has been observed to have cooled over the past decades [*Donaldson et al.*, 2010; *Zhang et al.*, 2011], we must conclude that the decreasing dipole moment actually acts against the main mechanism(s) responsible for this cooling trend, which has still not been fully explained [*Cnossen*, 2012]. However, the influence of the decreasing dipole moment is very small compared to the magnitude of typical observed trends (−30 to −50 K/decade). Changes in magnetic field strength therefore do not seem to be important in causing trends in global mean thermospheric temperature on a decadal to century timescale. And since at least part of the changes in h_mF_2 appears to be due to thermal expansion/contraction, we may expect the effects on global mean h_mF_2 to be relatively minor as well. Locally however, changes in magnetic field strength could still have a significant effect, as there are strong spatial variations in the patterns of change in both neutral temperature and h_mF_2 [*Cnossen et al.*, 2011].

[38] We also estimate changes in the Sq amplitude from 1910 to 2010 based on the scaling relations we found. This gives increases of 2.0–2.4, 3.0–4.7, and 1.3–2.0 nT, or 7.2–9.2, 6.2–6.8, and 6.3–6.8% in the northward, eastward, and downward Sq amplitude components, respectively. These values are slightly larger than the average upward trend of 1.3 nT/century reported by *Macmillan and Droujinina* [2007] or the 2.45 nT/century increase in the eastward component reported by *Svalgaard* [2009], but smaller than the trends of 4.8–8 nT/century reported by *Elias et al.* [2010]. Bearing in mind that actual trends are likely to vary from place to place, it appears that changes in dipole moment could make a significant contribution to long-term changes in Sq amplitude.

[39] *Svalgaard* [2009] noted that in particular the eastward component of the daily Sq variation is a useful indicator of solar activity, and may be used as a tool to calibrate the long-term sunspot number record. Clearly, if geomagnetic data are to be used in this way, the effects of the decreasing dipole moment on Sq variation must be considered and corrected for. Our scaling relations will be a first tool to do so, although local changes in the magnetic field over specific stations could also be important. Further work with more realistic magnetic field changes is needed to determine this more precisely. The fact that the scaling of the Sq amplitude

Table 1. Exponents γ for Power Law Scaling Relations of the Form [Variable] $\propto M^{\gamma}$ for the Stand-Off Distance, R_s, Mean Pedersen Conductance, Σ_P, Mean Hall Conductance, Σ_H, the Cosine of the Magnetic Latitude Boundary of the Polar Cap, cos λ_{pc}, and the Northward, Eastward, and Downward Components of the Sq Amplitude for Solar Minimum, Medium and Maximum Conditions[a]

	R_s	Σ_P	Σ_H	cos λ_{pc}	Sq North	Sq East	Sq Down
smin	0.43 ± 0.03	-1.3 ± 0.2	-1.5 ± 0.1	-0.25 ± 0.05	-1.22 ± 0.03	-0.90 ± 0.04	-0.91 ± 0.01
smed	0.45 ± 0.03	-1.5 ± 0.2	-1.5	-0.24 ± 0.03	-1.06 ± 0.08	-0.85 ± 0.04	-0.86 ± 0.05
smax	0.47 ± 0.02	-1.7 ± 0.2	-1.5	-0.22 ± 0.06	-0.97 ± 0.39	-0.82 ± 0.14	-0.84 ± 0.11
Theory	0.33	-1	-1.3	-0.17			

[a]The scaling coefficients given for the Sq amplitudes are valid for the range M4-M10 only, while all others are valid for the full range (M2-M10). Theoretical scaling exponents are also given where available. The theoretical scaling relations for Σ_P and Σ_H are from *Glassmeier et al.* [2004] and the one for cos λ_{pc} is from *Siscoe and Chen* [1975].

with M is in itself slightly dependent on solar activity could also complicate matters somewhat, although this effect is not very large for the range of dipole moments that needs to be considered.

5. Summary and Conclusions

[40] We derived new scaling laws for several magnetospheric and ionospheric variables with the geomagnetic dipole moment, based on simulations with a coupled magnetosphere-ionosphere-thermosphere model. These are summarized in Table 1. We generally find stronger scaling relations than previous theoretical and modeling studies have predicted. This is may be due to enhanced magnetopause erosion as the dipole moment decreases and/or to a strong increase in ionospheric conductance as the magnetic field weakens, which influences the field-aligned currents. These generate magnetic fields in the magnetosphere that add to the main field on the flanks, but oppose the main field on the nose, modifying the scaling of the stand-off distance with the dipole moment, as well as the shape of the magnetosphere. This feedback mechanism was not fully included in previous work.

[41] We examined for the first time how $\mathbf{E} \times \mathbf{B}$ drift velocities, Joule heating, global mean thermospheric temperature, and global mean N_mF_2 and h_mF_2 depend on the dipole moment. While the electric field E increases with increasing dipole moment, $\mathbf{E} \times \mathbf{B}$ drift velocities, which scale as E/B, increase with increasing dipole moment when the dipole moment is low and start decreasing when the dipole moment becomes higher (from 4 to $6 \cdot 10^{22}$ Am^2 onward, depending on the solar activity level). The Joule heating power, global mean thermospheric temperature, and h_mF_2 all follow this behavior. N_mF_2 behaves in the opposite sense: it initially shows a decrease with increasing dipole moment, but increases with increasing dipole moment for larger dipole moments. This is related to changes in circulation which modify the O/N_2 ratio.

[42] We also derived for the first time a scaling relation for the amplitude of the daily geomagnetic Sq variation with the dipole moment. A comparison with observed trends in Sq amplitudes indicated that changes in dipole moment could have contributed significantly to those trends.

[43] Most scaling relations show a weak dependence on the solar activity level, which is likely due to the solar activity dependence of the scaling for the Pedersen conductance. This arises from a change in the relative contributions to the Pedersen conductance from the upper and lower ionosphere, which depend differently on the magnetic field strength.

[44] **Acknowledgments.** We would like to thank Wenbin Wang for helpful comments on an earlier version of the manuscript. Part of this work was supported by NASA grants NNH07AF041 and NNX08AG09G. The National Center for Atmospheric Research is sponsored by the National Science Foundation.

[45] Robert Lysak thanks Leif Svalgaard and another reviewer for their assistance in evaluating this paper.

References

Cnossen, I. (2012), Climate change in the upper atmosphere, in *Greenhouse Gases: Emission, Measurement, and Management*, edited by G. Liu, pp. 315–336, InTech, Rijeka, Croatia, ISBN 978-953-51-0323-3.

Cnossen, I., and A. D. Richmond (2008), Modelling the effects of changes in the Earth's magnetic field from 1957 to 1997 on the ionospheric hmF2 and foF2 parameters, *J. Atmos. Sol. Terr. Phys.*, *70*(11–12), 1512–1524, doi:10.1016/j.jastp.2008.05.003.

Cnossen, I., A. D. Richmond, M. Wiltberger, W. Wang, and P. Schmitt (2011), The response of the coupled magnetosphere-ionosphere-thermosphere system to a 25% reduction in the dipole moment of the Earth's magnetic field, *J. Geophys. Res.*, *116*, A12304, doi:10.1029/2011JA017063.

Donaldson, J. K., T. J. Wellman, and W. L. Oliver (2010), Long-term change in thermospheric temperature above Saint Santin, *J. Geophys. Res.*, *115*, A11305, doi:10.1029/2010JA015346.

Elias, A. G., M. Zossi de Artigas, and B. F. de Haro Barbas (2010), Trends in the solar quiet geomagnetic field variation linked to the Earth's magnetic field secular variation and increasing concentrations of greenhouse gases, *J. Geophys. Res.*, *115*, A08316, doi:10.1029/2009JA015136.

Finlay, C. C., et al. (2010), International geomagnetic reference field: The eleventh generation, *Geophys. J. Int.*, *183*, 1216–1230, doi:10.1111/j.1365-246X.2010.04804.x.

Glassmeier, K.-H., J. Vogt, A. Stadelmann, and S. Buchert (2004), Concerning long-term geomagnetic variations and space climatology, *Ann. Geophys.*, *22*(10), 3669–3677, doi:10.5194/angeo-22-3669-2004.

Gubbins, D., A. L. Jones, and C. C. Finlay (2006), Fall in Earth's magnetic field is erratic, *Science*, *312*(5775), 900–902, doi:10.1126/science.1124855.

Guyodo, Y., and J.-P. Valet (1999), Global changes in intensity of the Earth's magnetic field during the past 800 kyr, *Nature*, *399*(6733), 249–252, doi:10.1038/20420.

Hill, T. W., A. J. Dessler, and R. A. Wolf (1976), Mercury and Mars: The role of ionospheric conductivity in the acceleration of magnetospheric particles, *Geophys. Res. Lett.*, *3*, 429–432, doi:10.1029/GL003i008p00429.

Kivelson, M. G., and C. T. Russell (1995), *Introduction to Space Physics*, 568 pp., Cambridge Univ. Press, Cambridge, U. K.

Lyon, J. G., J. A. Fedder, and C. M. Mobarry (2004), The Lyon-Fedder-Mobarry (LFM) global MHD magnetospheric simulation code, *J. Atmos. Sol. Terr. Phys.*, *66*(15–16), 1333–1350, doi:10.1016/j.jastp.2004.03.020.

Macmillan, S., and A. Droujinina (2007), Long-term trends in geomagnetic daily variation, *Earth Planets Space*, *59*, 391–395.

Mandea, M., and M. Purucker (2005), Observing, modelling, and interpreting magnetic fields of the solid Earth, *Surv. Geophys.*, *26*(4), 415–459, doi:10.1007/s10712-005-3857-x.

Merkin, V. G., and J. G. Lyon (2010), Effects of the low-latitude ionospheric boundary condition on the global magnetosphere, *J. Geophys. Res.*, *115*, A10202, doi:10.1029/2010JA015461.

Merkin, V. G., A. S. Sharma, K. Papadopoulos, G. Milikh, J. Lyon, and C. Goodrich (2005), Relationship between the ionospheric conductance,

field aligned current, and magnetopause geometry: Global MHD simulations, *Planet. Space Sci.*, *53*, 873–879, doi:10.1016/j.pss.2005.04.001.

Richmond, A. D. (1995), Ionospheric electrodynamics, in *Handbook of Atmospheric Electrodynamics*, vol. II, edited by H. Volland, pp. 249–290, CRC Press, Boca Raton, Fla.

Richmond, A. D., E. C. Ridley, and R. G. Roble (1992), A thermosphere/ionosphere general circulation model with coupled electrodynamics, *Geophys. Res. Lett.*, *19*(6), 601–604, doi:10.1029/92GL00401.

Roble, R. G., E. C. Ridley, A. D. Richmond, and R. E. Dickinson (1988), A coupled thermosphere/ionosphere general circulation model, *Geophys. Res. Lett.*, *15*(12), 1325–1328, doi:10.1029/GL015i012p01325.

Siscoe, G. L., and C.-K. Chen (1975), The paleomagnetosphere, *J. Geophys. Res.*, *80*(34), 4675–4680, doi:10.1029/JA080i034p04675.

Siscoe, G. L., G. M. Erickson, B. U. O. Sonnerup, N. C. Maynard, J. A. Schoendorf, K. D. Siebert, D. R. Weimer, W. W. White, and G. R. Wilson (2002a), Hill model of transpolar potential saturation: Comparisons with MHD simulations, *J. Geophys. Res.*, *107*(A6), 1075, doi:10.1029/2001JA000109.

Siscoe, G. L., N. U. Crooker, and K. D. Siebert (2002b), Transpolar potential saturation: Roles of region 1 current system and solar wind ram pressure, *J. Geophys. Res.*, *107*(A10), 1321, doi:10.1029/2001JA009176.

Svalgaard (2009), Observatory data: A 170-year Sun-Earth connection, *U.S. Geol. Surv. Open File Rep.*, *2009–1226*, 271 pp.

Tarduno, J. A., R. D. Cottrell, M. K. Watkeys, A. Hofmann, P. V. Doubrovine, E. E. Mamajek, D. Liu, D. G. Sibeck, L. P. Neukirch, and Y. Usui (2010), Geodynamo, solar wind, and magnetopause 3.4 to 3.45 billion years ago, *Science*, *327*, 1238–1240, doi:10.1126/science.1183445.

Wang, W., M. Wiltberger, A. G. Burns, S. C. Solomon, T. L. Killeen, N. Maruyama, and J. G. Lyon (2004), Initial results from the coupled magnetosphere-ionosphere-thermosphere model: Thermosphere-ionosphere responses, *J. Atmos. Sol. Terr. Phys.*, *66*(15–16), 1425–1441, doi:10.1016/j.jastp.2004.04.008.

Wang, W. B., J. H. Lei, A. G. Burns, M. Wiltberger, A. D. Richmond, S. C. Solomon, T. L. Killeen, E. R. Talaat, and D. N. Anderson (2008), Ionospheric electric field variations during a geomagnetic storm simulated by a coupled magnetosphere ionosphere thermosphere (CMIT) model, *Geophys. Res. Lett.*, *35*, L18105, doi:10.1029/2008GL035155.

Wiltberger, M., R. E. Lopez, and J. G. Lyon (2003), Magnetopause erosion: A global view from MHD simulation, *J. Geophys. Res.*, *108*(A6), 1235, doi:10.1029/2002JA009564.

Wiltberger, M., W. Wang, A. G. Burns, S. C. Solomon, J. G. Lyon, and C. C. Goodrich (2004), Initial results from the coupled magnetosphere ionosphere thermosphere model: Magnetospheric and ionospheric responses, *J. Atmos. Sol. Terr. Phys.*, *66*(15–16), 1411–1423, doi:10.1016/j.jastp.2004.03.026.

Wiltberger, M., R. S. Weigel, W. Lotko, and J. A. Fedder (2009), Modeling seasonal variations of auroral particle precipitation in a global-scale magnetosphere-ionosphere simulation, *J. Geophys. Res.*, *114*, A01204, doi:10.1029/2008JA013108.

Zhang, S.-R., J. M. Holt, and J. Kurdzo (2011), Millstone Hill ISR observations of upper atmospheric long-term changes: Height dependency, *J. Geophys. Res.*, *116*, A00H05, doi:10.1029/2010JA016414.

Zieger, B., J. Vogt, A. J. Ridley, and K. H. Glassmeier (2006a), A parametric study of magnetosphere-ionosphere coupling in the paleomagnetosphere, *Adv. Space Res.*, *38*, 1707–1712, doi:10.1016/j.asr.2005.04.077.

Zieger, B., J. Vogt, and K.-H. Glassmeier (2006b), Scaling relations in the paleomagnetosphere derived from MHD simulations, *J. Geophys. Res.*, *111*(A6), A06203, doi:10.1029/2005JA011531.